Soft Matter

Accepted Manuscript

ROYAL SOCIETY OF CHEMISTRY

www.rsc.org/softmatter

ARTICLE TYPE www. rsc.org/xxxxxx | XXXXXXXX

Equilibrium and nonequilibrium dynamics of soft sphere fluids†

Yajun Ding and Jeetain Mittal*

Received Xth XXXXXXXXXX 20XX, Accepted Xth XXXXXXXXX 20XX
First published on the web Xth XXXXXXXXXX 200X
DOI: 10.1039/b000000x

We use computer simulations to test the freezing-point scaling relationship between equilibrium transport coefficients (self-diffusivity, viscosity) and thermodynamic parameters for soft sphere fluids. The fluid particles interact via the inverse-power potential (IPP), and the particle softness is changed by modifying the exponent of the distance-dependent potential term. In the case of IPP fluids, density and temperature are not independent variables and can be combined to obtain a coupling parameter to define the thermodynamic state of the system. We find that the rescaled coupling parameter, based on its value at the freezing point, can approximately collapse the diffusivity and viscosity data for IPP fluids over a wide range of particle softness. Even though the collapse is far from perfect, the freezing-point scaling relationship provides a convenient and effective way to compare the structure and dynamics of fluid systems with different particle softness. We further show that an alternate scaling relationship based on two-body excess entropy can provide an almost perfect collapse of the diffusivity and viscosity data below the freezing transition. Next, we perform nonequilibrium molecular dynamics simulations to calculate the shear-dependent viscosity and to identify the distinct role of particle softness in underlying structural changes associated with rheological properties. Qualitatively, we find a similar shear-thinning behavior for IPP fluids with different particle softness, though softer particles exhibit stronger shear-thinning tendency. By investigating the distance and angle-dependent pair correlation functions in these systems, we find different structural features in the case of IPP fluids with hard-sphere like and softer particle interactions. Interestingly, shear-thinning in hard-sphere like fluids is accompanied by enhanced translational order, whereas softer fluids exhibit loss of order with shear. Our results provide a systematic evaluation of the role of particle softness in equilibrium and nonequilibrium transport properties and their underlying connection with thermodynamic and structural properties.

1 Introduction

Concentrated suspensions of soft particles, such as microgel suspensions, polymer coated colloids and compressed oil in water emulsions, have attracted a lot of scientific interest[1,2]. These soft particles which are deformable and impenetrable can be packed beyond the random close packing fraction for hard spheres[3]. Purely repulsive inter-particle interactions have been widely used to model soft particle suspensions and to understand the fundamental questions related to their behavior[4,5]. Among various soft repulsive potentials, the inverse-power potential (IPP) has been studied extensively due to its simple form and ability to capture interesting physical phenomenon[6–10]. For large values of n, the behavior of the IPP approaches the hard sphere limit[11]. The interactions between poly-12-hydroxystearic acid (PHSA) particles[4] and several types of core-shell microgel particles[5,12–14] have been successfully mapped to the IPP. The IPP model has simply two phases: the fluid phase and the crystal phase, with a well-known universal phase diagram[15–17]. The thermodynamic state of an IPP fluid is governed by a single dimensionless parameter that couples the temperature and density.

The relationship between particle softness and the static and dynamic properties has been a major topic of interest for soft particles[18,19]. Recent simulations of IPP fluids attempted to establish the scaling relation between the transport coefficients (e.g., diffusion coefficient or viscosity) and the particle softness. A scaling law derived from the perturbation theory was proposed to collapse transport coefficients for extremely soft systems ($n \leq 12$), while it was deemed ineffective for higher n due to the lack of higher order terms in the expansion of the interaction energy[20]. More recently, for intermediate n ($18 \leq n \leq 36$), a scaling relation based on the freezing point is able to collapse the transport coefficients[21]. In addition to the scaling relations specifically for the IPP, Rosenfeld proposed a simple quasi-universal relationship between reduced transport coefficients and excess entropy[22]. This relationship is supported by many studies on various fluid models[23,24] and real fluids[25,26].This treatment has also been extended to binary fluid mixtures[23,26–28], anomalies in water-like model fluids[29–38] and particles under confinement[39,40].

In the first part of this paper, we test the freezing-point scaling relation for soft sphere fluids for an extended parametric space ($n \geq 4$) through molecular dynamics simulations. We

† Electronic Supplementary Information (ESI) available: See DOI: 10.1039/b000000x/

Department of Chemical and Biomolecular Engineering, Lehigh University, Bethlehem, Pennsylvania 18015, USA. E-mail: jeetain@lehigh.edu

find that the reduced diffusion coefficient and viscosity data for IPP fluids collapse when plotted against the reduced coupling parameter for a broader set of potential softness; the quality of the collapse deteriorates away from the freezing transition. We also report data to test the scaling relation between the reduced transport coefficients and the two-body excess entropy. An almost perfect collapse of all the data below the freezing transition is observed in this case, which further highlights the usefulness of entropy-based scaling relationships.

Colloidal suspensions exhibit nonlinear response to the applied flow rate, i.e., shear thinning, thickening or a combination of the two types of responses. Understanding the shear rheology of dense colloidal suspensions still remains a challenge. Many experimental studies and computer simulations have attempted to relate changes in particle configurations to the nonlinearity of these phenomena[41–50]. Recently, simultaneous appearance of layering and shear thinning was observed by Cheng et al.[43]. However the results of Xu et al.[51] indicated that the simultaneous appearance of layering and shear thinning is coincidental rather than causal. They demonstrated that pair structure in the suspension has a stronger correlation with shear-thinning phenomenon, whereas the layer formation can be enhanced by the presence of planar boundaries, e.g., walls in experiments or simulations[51]. Several groups observed hydroclusters in the shear thickening regime[43,45], which is consistent with the prediction by Brady and coworkers[52–55] that shear thickening is caused by the formation of transient hydroclusters induced by shearing.

Shear rheology of hard sphere systems, such as silica, polymethyl-methacrylate (PMMA) and polystyrene (PS), have been extensively studied due to its simplicity and abundance of relevant theoretical work[56,57]. Soft sphere systems, spanning from ultrasoft polymeric coils and star polymers such as core-shell microgels and emulsions, show richer rheological behavior than their hard sphere counterparts[1–3]. Understanding and predicting the relation between structure and macroscopic rheological properties of soft sphere fluids is much more challenging. The rheological properties of soft particle systems are closely linked to the interparticle interaction softness, which implies the tunability of the rheological behavior by varying the particle softness. Nazockdast and Morris[58] investigated the effect of steepness of repulsive interactions on the structure and rheology of sheared colloidal suspensions from both simulations and theory. In their study, soft colloids, modeled by a combination of hard-sphere and Yukawa interaction potentials, exhibited only the shear-thinning behavior and lack of shear thickening. They proposed that lubrication forces are significantly reduced in soft colloidal systems, and the interparticle repulsive force balances the shearing force to determine the pair microstructure. Recently, Zhou et al.[12] examined the effect of microgel softness on its shear thickening behavior using core-shell microgel particles. The measured interaction potentials between microgel particles were successfully mapped to the inverse-power potential. With an increase in the effective volume fraction or temperature, or decrease in the shell thickness, the shear thickening behavior became more obvious. Xu et al.[41] also examined the effect of particle softness on the structure of colloidal suspension by tuning electrostatic interactions, which effectively changes the particle diameter, thereby affecting the direct contact distance between the particles. They found that electrostatic interactions played a complex role in the suspension structure.

In the second part of this paper, we investigate the effect of particle softness on the microstructure and rheology of soft sphere fluids using nonequilibrium molecular dynamics (NEMD) simulations. Qualitatively, we observe a similar shear-thinning behavior for particles with different softness, though softer particles exhibit stronger shear-thinning tendency. By investigating the microstructure of these systems, we find a strong correlation between the structural changes and particle softness in the presence of shear. Specifically, shear slightly enhances the overall translational order of quasi hard-sphere fluids by strengthening correlations between nearest-neighbor particles, while significantly decreasing the translational order in the case of softer particles by weakening the long-range correlations. Shear has a more pronounced effect on enhancing the correlation along the flow direction for quasi-hard sphere fluids, while inducing a pronounced secondary depletion region for ultrasoft particles. These different responses to shear can explain the extent of shear-thinning behavior observed for different particle softness.

2 Model and methods

The soft sphere potential has the form:

$$U(r) = \varepsilon \left(\frac{\sigma}{r}\right)^n, \tag{1}$$

where r is the distance between two particles, σ is the particle diameter, ε sets the energy scale and n determines the increasing particle softness with decreasing n. Throughout this paper we use reduced Lennard-Jones (LJ) units, where σ is the unit of distance, ε is the unit of energy, and mass is measured in units of particle mass m. The cutoff distance is set to $r_c = 2.5\sigma$. We simulate a system of 500 particles in a canonical ensemble (constant N, V, and T) using the Nosé-Hoover thermostat[59]. Equations of motion are integrated using the velocity Verlet algorithm with a time step of 0.001 in reduced LJ units. Because the thermodynamic state of IPP fluid is governed by the coupling parameter $\Gamma = \rho\sigma^3(\varepsilon/k_BT)^{3/n}$, where ρ is the number density, k_B is Boltzmann's constant and T is the absolute temperature, the density and temperature essentially

play the same role. In this study we set $T = 1.0$ for simplicity. The state points employed in simulations and values of the coupling parameter at the freezing point, Γ_f, for different particle softness n are tabulated in Table S1†. The initial configuration is an fcc lattice, which is first melted at very high temperature ($T = 4.0$), and then the system temperature is quenched to the temperature $T = 1.0$ for further equilibration. The diffusion coefficients are calculated from the mean square displacement via the Einstein relation[60], while the zero-shear viscosity is determined by using the Green-Kubo relation[61]. For NEMD simulations, the thermostatted SLLOD equations of motion with continuous deformation of the box shape, which is conceptually similar to the Lees-Edwards boundary condition, are used to study the system under shear[62]. The x-direction is set as the flow direction, while the velocity gradient is applied in the y-direction. Shear rate is defined as $\dot{\gamma} = dv_x/dy$, and the shear viscosity is calculated as $\eta = \langle \Sigma_{xy} \rangle / \dot{\gamma}$, where Σ_{xy} is the xy component of the stress tensor. The two-body translational structural order parameter or excess entropy s_2 is computed using the expression[63]:

$$s_2 = -\frac{\rho}{2} \int \{g(\mathbf{r}) \ln g(\mathbf{r}) - [g(\mathbf{r}) - 1]\} d\mathbf{r}, \qquad (2)$$

where ρ is the number density and $g(\mathbf{r})$ is the pair distribution function. This expression stems from an expansion of entropy in terms of the partial N-body distribution functions[64,65]. s_2 is zero for completely disordered systems, and becomes negative infinity for a perfect crystal. Although excess entropy can be rigorously calculated via simulations[28,40,64], it has been shown in earlier studies that the two-body excess entropy is a reasonable approximation for the full excess entropy in the case of many atomistic fluids[23,24]. The cumulative order integral I_{s_2} is defined as:

$$I_{s_2}(r) = \frac{\rho}{2} \int_0^r dr' \int_0^{2\pi} d\theta \int_0^{\pi} d\phi r'^2 sin(\phi) f(r', \theta, \phi), \qquad (3)$$

where $f(r', \theta, \phi) = g(r', \theta, \phi) \ln g(r', \theta, \phi) - [g(r', \theta, \phi) - 1]$. I_{s_2} measures how interparticle correlations on length scales less than r impact the structural order. As defined, I_{s_2} approaches -s_2 as r approaches ∞.

3 Results and discussion

3.1 Equilibrium transport coefficients

Lange et al.[21] proposed a scaling law based on the coupling parameter at the freezing point, Γ_f, to scale the diffusion coefficient and viscosity data for $n \geq 18$. They observed that the long-range structure is almost identical for systems with different particle softness at the freezing point, while structural differences at short distances appeared because of the different shapes of the interaction potential. The reduced coupling parameter Γ/Γ_f basically measures how far the system is away from the freezing transition, which can be treated as a key parameter for comparing systems with different softness. In this study, we first test this scaling law for an extended parametric space. Specifically, we investigate n = 4, 6, 8, 10, 12, 24, 36 and $0.01 \leq \Gamma/\Gamma_f \leq 1$.

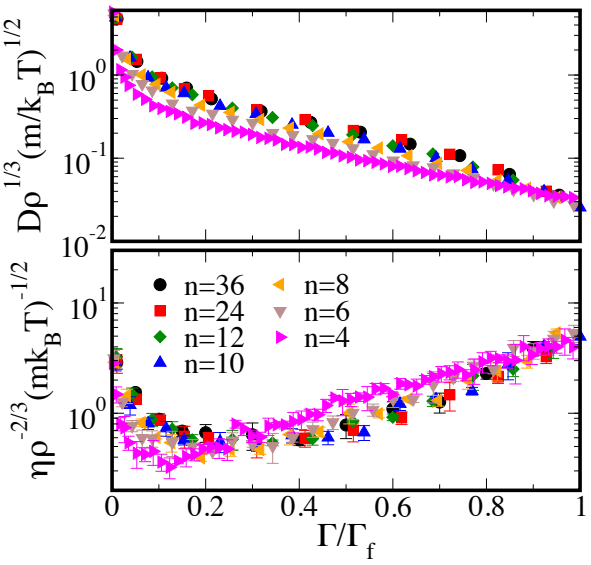

Fig. 1 (top panel) Reduced diffusion coefficient, $D\rho^{1/3}(k_BT/m)^{-1/2}$, and (bottom panel) reduced viscosity, $\eta\rho^{-2/3}(mk_BT)^{-1/2}$, versus reduced coupling parameter Γ/Γ_f for different particle softness, n, as indicated in the legend.

We use the reduced transport coefficients, $D^* = D\rho^{1/3}(k_BT/m)^{-1/2}$ and $\eta^* = \eta\rho^{-2/3}(mk_BT)^{-1/2}$ as suggested by Rosenfeld[22] to account for trivial changes in D and η due to temperature and density. Figure 1 shows the reduced diffusion coefficient, D^* (top panel), and viscosity, η^* (bottom panel), as a function of the reduced coupling parameter Γ/Γ_f for different particle softness, n. The unscaled D and η data are plotted as a function of Γ and Γ/Γ_f in Figures S1 and S2†. Both D^* and η^* appear to collapse onto single curves when plotted versus Γ/Γ_f. Although the scaling law leads to a collapse of both diffusion and viscosity data, one can notice that the width of the master curve is still large. Due to the large statistical uncertainty in estimating viscosity, the master curve for viscosity is thicker than that for diffusion. The quality of the collapse improves with increasing n as the system approaches the hard-sphere limit. Also, as the density (or Γ) increases and approaches freezing, the quality of the collapse improves in both cases as one might expect.

Another useful thermodynamic quantity that can also be measured easily in a simulation is the two-body excess entropy s_2[66]. Rosenfeld[22] observed that reduced transport coefficients exponentially depend on the excess entropy of a liquid.

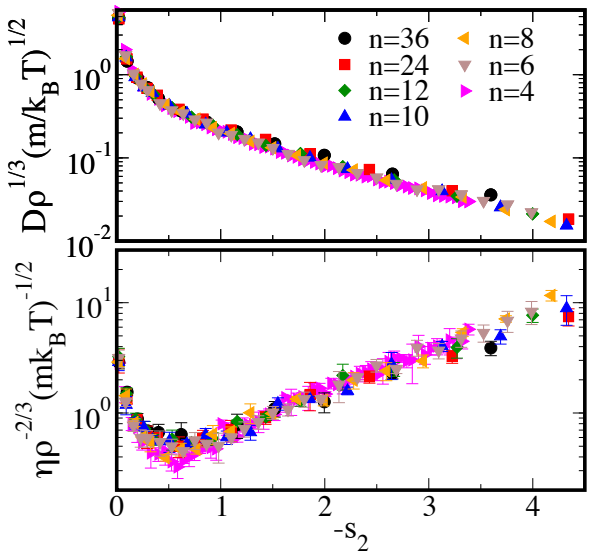

Fig. 2 (top panel) Reduced diffusion coefficient, $D\rho^{1/3}(k_BT/m)^{-1/2}$, and (bottom panel) reduced viscosity $\eta\rho^{-2/3}(mk_BT)^{-1/2}$, versus negative two-body excess entropy, $-s_2$, for different softness, n, as indicated in the legend.

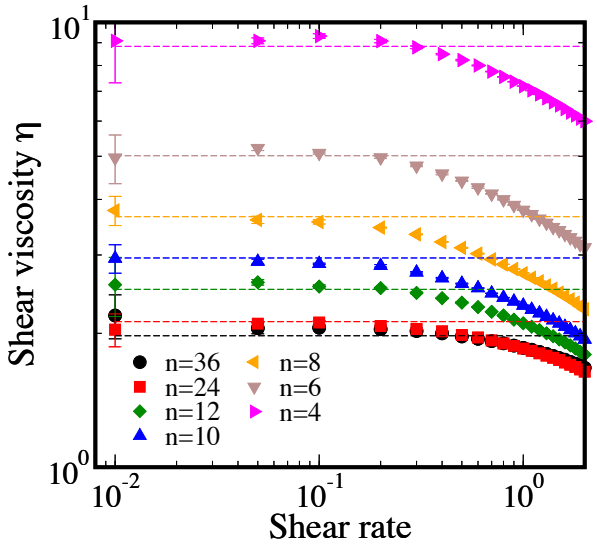

Fig. 3 Shear viscosity η versus shear rate $\dot{\gamma}$ for the different particle softness n described in the legend at $\Gamma/\Gamma_f = 0.85$. Dashed lines represent zero-shear viscosity η_0.

In fact, this relation is approximately true for many "strongly correlating" simple liquids[67].

The quantitative link between the reduced transport coefficient and $-s_2$ is tested here for soft sphere fluids. Figure 2 shows the reduced diffusion coefficient D^* (top panel) and viscosity η^* (bottom panel) data as a function of $-s_2$ for different particle softness n (see legend). Both D^* and η^* appear to collapse onto narrow single master curves when plotted versus $-s_2$, with a significantly better quality of collapse than the scaling based on Γ/Γ_f. Our results clearly indicate that both Γ/Γ_f and s_2 correlate well with the transport coefficients when systems are near the freezing transition, while s_2 plays a better role even away from the freezing transition.

3.2 Nonequilibrium structure and dynamics

3.2.1 Rheological properties. As shown in the previous section, by maintaining equal Γ/Γ_f, systems with different particle softness have similar equilibrium dynamics near the freezing transition. Therefore, we select the state points close to the freezing transition, $\Gamma/\Gamma_f = 0.85$, for the shear simulations. The shear rate dependence of $\eta(\dot{\gamma})$ for different particle softness is shown in Figure 3. The extrapolation of the finite shear rate values to zero shear rate are consistent with the values obtained from the Green-Kubo relation as shown by horizontal dashed lines. The rheological behavior is Newtonian at low shear rates, where η approaches its zero-shear viscosity value η_0. At high shear rates, shear-thinning is observed in all cases. We note that the shear-thinning behavior is dependent on the softness of particle interactions even by maintaining the same Γ/Γ_f; softer particles exhibit stronger shear-thinning tendency.

We have also calculated the first and second normal stress difference as a function of the shear rate. First and second normal stress differences are defined as $N_1 = \Sigma_{xx} - \Sigma_{yy}$ and $N_2 = \Sigma_{yy} - \Sigma_{zz}$, which are both zero at equilibrium (zero shear) and become nonzero under shear[68]. As can be see in Figure 4, the sign of N_2 is negative for both $n = 36$ and 4 under shear, while N_1 is positive for $n = 4$ and slightly negative for $n = 36$ (see Figure S3 for other n values). The finding $N_1 > 0$ and $N_2 < 0$ for ultrasoft particles is consistent with previous results for charged colloids[69]. The finding $N_1, N_2 < 0$ for quasi hard-sphere particles resembles hard sphere behavior[54]. In addition, we also observe that an increase in particle softness (n from 36 to 4) leads to a more positive first normal stress difference (data not shown).

3.2.2 Microstructure. In order to investigate how particle softness relates to the changes in fluid structure under steady shear, pair distribution functions (PDF), $g(x,y)$, in the shear plane (x-y plane) were calculated for each of the systems for different shear rates. Figure 5 shows $g(x,y)$ for $n = 36$ (left) and 4 (right). For better contrast, upper cut-off values are imposed at $g(x,y) = 4$ and 6 for $n = 4$ and 36, respectively. At low shear rate, the structure is nearly isotropic and no angular variations are observed in the first and second nearest-neighbor rings. As the shear rate increases, there is a buildup of particles in the compressive axis ($\theta \approx 135°$) and a depletion of particles in the extensional axis ($\theta \approx 45°$) at $\dot{\gamma} = 1.0$

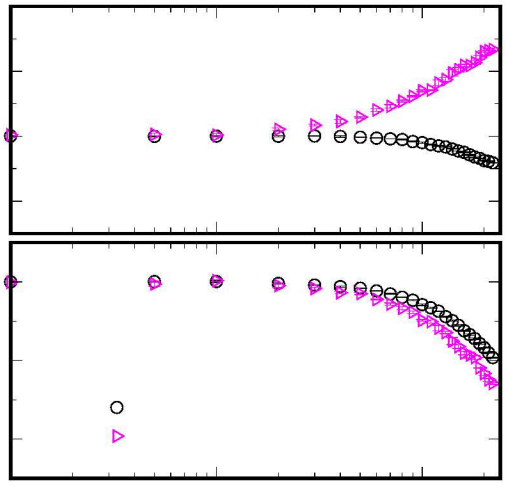

Fig. 4 First normal stress difference, N_1, and second normal stress difference, N_2, as function of shear rate for $n = 36$ and 4.

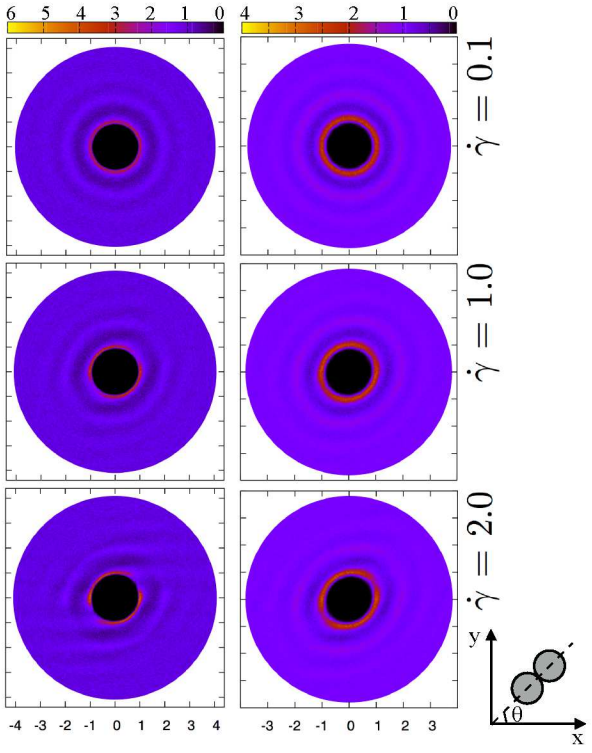

Fig. 5 Pair distribution function, $g(x,y)$, for $n = 36$ (left column) and 4 (right column) in the shear plane (x-y plane) at different shear rates $\dot{\gamma}$.

for both $n = 36$ and 4. This oval-like structure is initially symmetrical along the compressive axis. As the shear rate is further increased, the symmetry is broken by the appearance of diffusive tails near the opening of the innermost ring. This highlights convection of particles downstream into the neighboring extensional region as shown by high probability at 0° and 180° that indicate strong correlations along the flow direction. In addition, by comparing the two cases, the ultrasoft particles ($n = 4$) show thicker rings than quasi hard-sphere particles ($n = 36$), and the deformation of these rings with respect to shear rate for ultrasoft particles is not as significant as in the case of quasi hard-sphere particles.

To relate the shear-induced anisotropy to the particle softness, angularly averaged PDFs, $g_s(r)$, are shown as a function of shear rate, $\dot{\gamma}$, for $n = 36$ and 4 in Figure 6 (top panels). For $n = 36$, we observe a slightly sharpened nearest-neighbor peak and weakened second and third peaks with increasing shear rate. For $n = 4$, the effect of shear on $g_s(r)$ is to weaken both the short-range and long-range order as all the peaks are reduced with increasing shear rate. To quantify the subtle changes in order, we estimate the cumulative structural order, I_{s_2}, as shown in Figure 6 (bottom panels). As indicated by the downshift and flattening of the I_{s_2} curves in Figure 6, the contribution of multiple peaks to the overall structural order becomes less pronounced with increasing shear for ultrasoft particles ($n = 4$). For quasi hard-sphere particles ($n = 36$), the enhanced first peak makes a significant contribution to the overall structural order with increasing shear; I_{s_2} curves are almost parallel beyond the nearest-neighbor peak distance.

For a better illustration of the first peak variation in $g_s(r)$ under shear, the angular variation of PDF at the distance where the first peak in $g_s(r)$ is located, $g(r_c,\theta)$ are shown in Figure 7. For $n = 36$, insignificant deviations from equilibrium values ($\dot{\gamma} = 0$) are found for $\dot{\gamma} = 0.01$ and 0.1. For $\dot{\gamma} = 1.0$, $g(r_c,\theta)$ displays an approximately sinusoidal variation around the isotropic values, with the maximum and minimum approximately located at $\theta = 130°$ and 40°, respectively. For $\dot{\gamma} = 2.0$, secondary maximum and minimum are found at $\theta = 115°$ and 150°, respectively, with a deeper depleted correlation region at $\theta = 40°$ and enhanced correlations in the flow direction. The correlations along the flow direction become more pronounced as the shear rate is further increased, concomitant with the appearance of clear primary and secondary depletion regions.

For ultrasoft particles ($n = 4$), although similar changes in $g(r_c,\theta)$, relative to the equilibrium values, can be observed under shear, the differences from quasi hard-sphere particles ($n = 36$) are also apparent. For $\dot{\gamma} = 1.0$, there is no symmetrically distributed variation around the minimum and maximum values of $g(r_c,\theta)$. Instead a pair of minima are found at $\theta = 40°$ and $\theta = 150°$. The enhanced correlations along the flow direction due to shear become less pronounced as com-

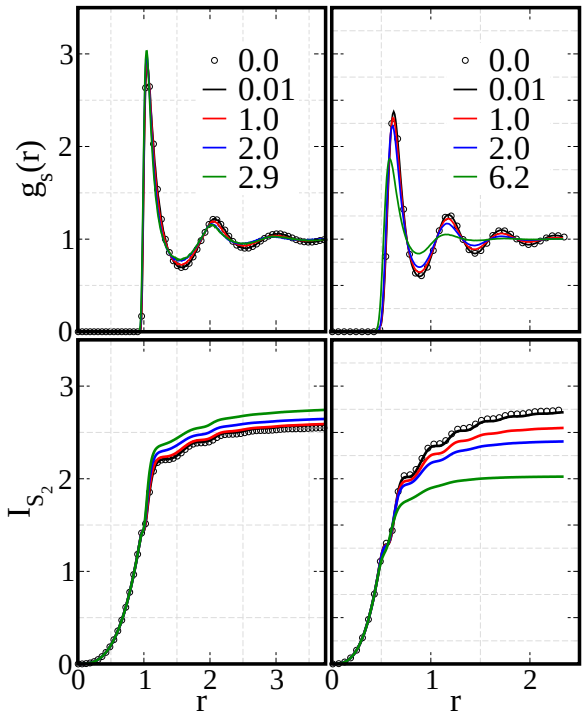

Fig. 6 (Top panels) Angularly averaged pair distribution function $g_s(r)$ for $n = 36$ (left column) and $n = 4$ (right column) at several shear rates, $\dot{\gamma}$. (Bottom panels) Calculated cumulative order integral, $I_{s_2}(r)$, corresponds to top panels.

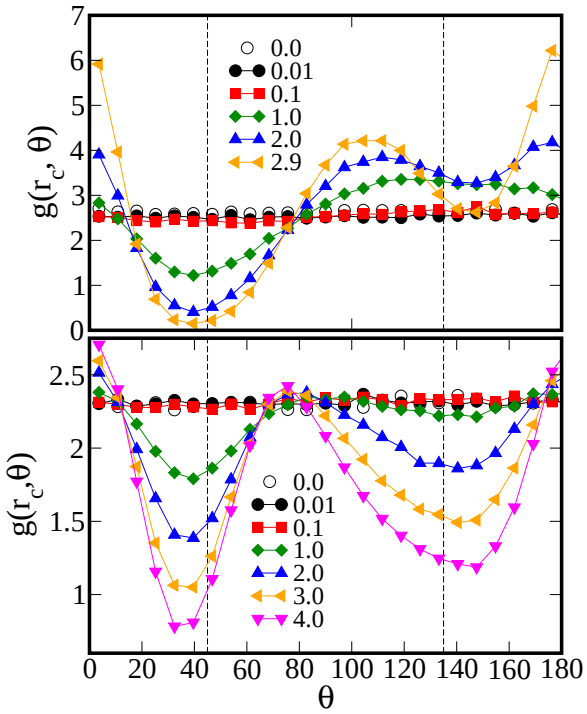

Fig. 7 Angular variation of PDF, $g(r_c, \theta)$, at the distance of the first peak of $g_s(r)$ for the particle softness $n = 36$ (upper) and 4 (bottom).

pared to $n = 36$. The contact values at $\theta = 40^\circ$ and 150° are found to decrease with increasing shear rate.

To summarize, the area under the $g(r_c, \theta)$ curve is slightly increased with shear for $n = 36$, while the corresponding area is clearly decreased with shear for $n = 4$. The weakened first peak for $n = 4$ is closely related to the formation of a secondary depletion region at $\theta = 150^\circ$ and to the weaker correlations along the flow direction. These observations help understand the structural changes underlying enhanced shear thinning in the case of softer particles.

Figure 8 summarizes the effect of shear on the translational structural order for different particle softness by comparing shear viscosity with -s_2, the latter of which is calculated based on $g_s(r)$. The data in Figure 8 suggest that the effect of shear for lower n, $n = 12, 10, 8, 6$ and 4, is to monotonically decrease both viscosity and translational order. In the case of higher n, $n = 24$ and 36, shear appears to decrease the viscosity but slightly increase the translational order. Recent simulations have also shown that the average translational structural order is weakened with increasing shear for fluid particles interacting with the Debye-Huckel repulsive potential[53], while enhanced nearest-neighbor correlations were found for hard-sphere suspensions[70]. Even though hydrodynamic interactions (HIs) were included in these previous simulations, we also observe similar behavior in the absence of HIs, which suggests that HIs do not alter the qualitative dependence of the translational order as a function of shear rate. We note that when HIs are considered, enhanced nearest-neighbor correlations for quasi hard-sphere particles can facilitate the formation of hydroclusters, which was confirmed in previous experiments[43,45] and simulations[52–55] as the main cause of shear thickening. For softer particles, decayed nearest-neighbor correlations tend to suppress the formation of hydroclusters, and, therefore, the difficulty in observing shear thickening.

4 Conclusions

In this paper, we test the freezing-point scaling relation for soft particle fluids over a broad range of particle softness. The freezing-point scaling relation, to a good approximation, can adequately collapse diffusivity and viscosity data for different particle softness. The freezing-point scaling relation is, therefore, a convenient and effective parameter for comparing the structure and dynamics of the system with different softness, especially when these systems are close to the freezing transition.

We apply the freezing-point scaling relation as a reason-

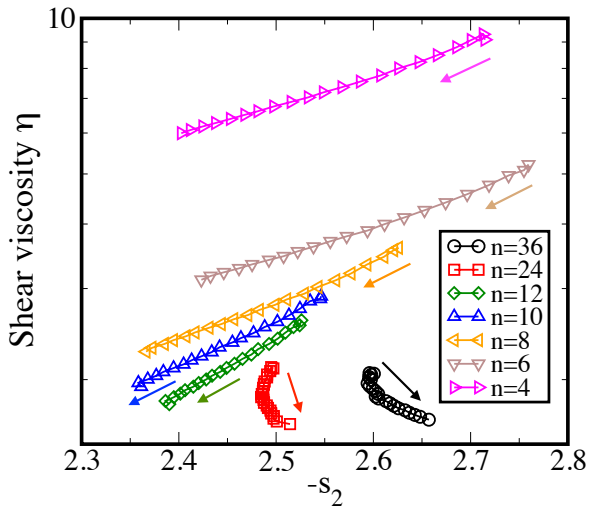

Fig. 8 Shear viscosity, η, versus order parameter, $-s_2$, for particles with different softness, n. Arrow indicates increasing shear rate.

able starting point to study the shear rheology and the microstructure of particles with different softness using NEMD simulations. Our results show a similar shear thinning behavior for particles with different softness, though softer particles exhibit stronger shear thinning tendency. By investigating the microstructure of these systems, we find that shear slightly enhances the overall translational order in quasi hard-sphere fluids by strengthening the correlations between nearest-neighbor particles, and by slightly weakening the long-range ordering, while significantly decreasing the order in the case of softer particles. By examining the angular variation of the pair distribution function, we find that shear has a more pronounced effect on enhancing the correlations along the flow direction for quasi hard-sphere fluids, while at the same time inducing a pronounced secondary depletion region for ultrasoft particles. The strong correlation between the structural changes and the particle softness in the presence of shear might explain the extent of shear thinning behavior for different particle softness.

5 Acknowledgments

We thank Prof. James F. Gilchrist (Lehigh University) for helpful discussions and comments on an earlier draft of this manuscript. This work was supported by the National Science Foundation (NSF) (Grant No. CBET-1120399). Use of the high-performance computing capabilities of the Extreme Science and Engineering Discovery Environment (XSEDE), which is supported by the NSF (Grant No. TG-MCB-120014), is also gratefully acknowledged.

References

1 D. Vlassopoulos and M. Cloitre, *Curr. Opin. Colloid Interface Sci.*, 2014, **19**, 561–574.
2 R. G. Winkler, D. A. Fedosov and G. Gompper, *Curr. Opin. Colloid Interface Sci.*, 2014, **19**, 594–610.
3 D. T. N. Chen, Q. Wen, P. A. Janmey, J. C. Crocker and A. G. Yodh, *Annu. Rev. Condens. Matter Phys.*, 2010, **1**, 301–322.
4 G. Bryant, S. Williams, L. Qian, I. Snook, E. Perez and F. Pincet, *Phys. Rev. E*, 2002, **66**, 060501.
5 C. P. Royall, W. C. K. Poon and E. R. Weeks, *Soft Matter*, 2013, **9**, 17–27.
6 A. C. Branka and D. M. Heyes, *Phys. Rev. E*, 2006, **74**, 031202.
7 D. M. Heyes and A. C. Branka, *Phys. Chem. Chem. Phys.*, 2007, **9**, 5570–5575.
8 D. M. Heyes and A. C. Branka, *Phys. Chem. Chem. Phys.*, 2008, **10**, 4036–4044.
9 D. M. Heyes and A. C. Branka, *J. Phys.-Condes. Matter*, 2008, **20**, 115102.
10 D. M. Heyes and A. C. Branka, *Mol. Phys.*, 2009, **107**, 309–319.
11 D. Heyes and A. Branka, *J. Chem. Phys.*, 2005, **122**, 234504.
12 Z. Zhou, J. V. Hollingsworth, S. Hong, G. Wei, Y. Shi, X. Lu, H. Cheng and C. C. Han, *Soft Matter*, 2014, **10**, 6286–6293.
13 N. Koumakis, A. Pamvouxoglou, A. S. Poulos and G. Petekidis, *Soft Matter*, 2012, **8**, 4271–4284.
14 H. Senff, W. Richtering, C. Norhausen, A. Weiss and M. Ballauff, *Langmuir*, 1999, **15**, 102–106.
15 R. Agrawal and D. A. Kofke, *Mol. Phys.*, 1995, **85**, 23–42.
16 S. Khrapak and G. Morfill, *Phys. Rev. Lett.*, 2009, **103**, 255003.
17 S. Prestipino, F. Saija and P. V. Giaquinta, *J. Chem. Phys.*, 2005, **123**, 144110.
18 H. C. Andersen, J. D. Weeks and D. Chandler, *Phys. Rev. A*, 1971, **4**, 1597–1607.
19 D. Ben-Amotz and G. Stell, *J. Chem. Phys.*, 2004, **120**, 4844–4851.
20 Y. Rosenfeld and P. Tarazona, *Mol. Phys.*, 1998, **95**, 141–150.
21 E. Lange, J. B. Caballero, A. M. Puertas and M. Fuchs, *The Journal of Chemical Physics*, 2009, **130**, –.
22 Y. Rosenfeld, *Phys. Rev. A*, 1977, **15**, 2545–2549.
23 M. Dzugutov, *Nature*, 1996, **381**, 137–139.
24 Y. Rosenfeld, *J. Phys.: Condens. Matter*, 2000, **10**, 129–134.
25 I. Yokoyama, *Physica B: Condens. Matter*, 1998, **254**, 172–177.
26 Y. Rosenfeld, E. Nardi and Z. Zinamon, *Phys. Rev. Lett.*, 1995, **75**, 2490–2493.
27 J. Hoyt, M. Asta and B. Sadigh, *Phys. Rev. Lett.*, 2000, **85**, 594–597.
28 J. Mittal, V. K. Shen, J. R. Errington and T. M. Truskett, *J. Chem. Phys.*, 2007, **127**, 154513.
29 J. R. Errington and P. G. Debenedetti, *Nature*, 2001, **409**, 318–321.
30 M. Shell, P. Debenedetti and A. Panagiotopoulos, *Phys. Rev. E*, 2002, **66**, 011202.
31 J. R. Errington, T. M. Truskett and J. Mittal, *J. Chem. Phys.*, 2006, **125**, 244502.
32 W. P. Krekelberg, J. Mittal, V. Ganesan and T. M. Truskett, *Phys. Rev. E*, 2008, **77**, 041201.
33 A. B. de Oliveira, G. Franzese, P. A. Netz and M. C. Barbosa, *The Journal of Chemical Physics*, 2008, **128**, –.
34 R. Sharma, S. N. Chakraborty and C. Chakravarty, *The Journal of Chemical Physics*, 2006, **125**, –.
35 M. Agarwal, M. Singh, R. Sharma, M. Parvez Alam and C. Chakravarty, *The Journal of Physical Chemistry B*, 2010, **114**, 6995–7001.
36 M. Agarwal, M. P. Alam and C. Chakravarty, *The Journal of Physical Chemistry B*, 2011, **115**, 6935–6945.
37 Y. D. Fomin, E. N. Tsiok and V. N. Ryzhov, *Phys. Rev. E*, 2013, **87**, 042122.

38 V. V. Vasisht, J. Mathew, S. Sengupta and S. Sastry, *The Journal of Chemical Physics*, 2014, **141**, –.

39 J. Mittal, J. R. Errington and T. M. Truskett, *Phys. Rev. Lett.*, 2006, **96**, 177804.

40 J. Mittal, J. R. Errington and T. M. Truskett, *J. Phys. Chem. B*, 2007, **111**, 10054–10063.

41 B. Xu and J. F. Gilchrist, *J. Chem. Phys.*, 2014, **140**, 204903.

42 C. Gao, S. Kulkarni, J. Morris and J. Gilchrist, *Phys. Rev. E*, 2010, **81**, 041403.

43 X. Cheng, J. H. McCoy, J. N. Israelachvili and I. Cohen, *Science*, 2011, **333**, 1276–1279.

44 X. Cheng, X. Xu, S. A. Rice, A. R. Dinner and I. Cohen, *Proc. Natl. Acad. Sci.*, 2012, **109**, 63–67.

45 D. Kalman and N. Wagner, *Rheol. Acta*, 2009, **48**, 897–908.

46 N. Y. C. Lin, S. Goyal, X. Cheng, R. N. Zia, F. A. Escobedo and I. Cohen, *Phys. Rev. E*, 2013, **88**, 062309.

47 N. Y. C. Lin, X. Cheng and I. Cohen, *Soft Matter*, 2014, **10**, 1969–1976.

48 L. Separdar, N. P. Bailey, T. B. Schrøder, S. Davatolhagh and J. C. Dyre, *The Journal of Chemical Physics*, 2013, **138**, –.

49 W. P. Krekelberg, V. Ganesan and T. M. Truskett, *Phys. Rev. E*, 2008, **78**, 010201.

50 W. P. Krekelberg, T. M. Truskett and V. Ganesan, *Chemical Engineering Communications*, 2009, **197**, 63–75.

51 X. l. Xu, S. A. Rice and A. R. Dinner, *Proc. Natl. Acad. Sci.*, 2013, **110**, 3771–3776.

52 T. N. Phung, J. F. Brady and G. Bossis, *J. Fluid Mech.*, 1996, **313**, 181–207.

53 G. Bossis, J. F. Brady and C. Mathis, *J. Colloid Interface Sci.*, 1988, **126**, 1–15.

54 D. R. Foss and J. F. Brady, *J. Fluid Mech.*, 2000, **407**, 167–200.

55 J. F. Brady and G. Bossis, *J. Fluid Mech.*, 1985, **155**, 105–129.

56 J. F. Morris, *Rheol. Acta*, 2009, **48**, 909–923.

57 J. J. Stickel and R. L. Powell, *Annu. Rev. Fluid Mech.*, 2005, **37**, 129–149.

58 E. Nazockdast and J. F. Morris, *Soft Matter*, 2012, **8**, 4223–4234.

59 W. Shinoda, M. Shiga and M. Mikami, *Phys. Rev. B*, 2004, **69**, 134103.

60 C. McCabe, C. W. Manke and P. T. Cummings, *J. Chem. Phys.*, 2002, **116**, 3339–3342.

61 P. J. Daivis and D. J. Evans, *J. Chem. Phys.*, 1994, **100**, 541–547.

62 D. J. Evans and G. P. Morriss, *Phys. Rev. A*, 1984, **30**, 1528–1530.

63 T. Truskett, S. Torquato and P. Debenedetti, *Phys. Rev. E*, 2000, **62**, 993–1001.

64 A. Baranyai and D. Evans, *Phys. Rev. A*, 1989, **40**, 3817–3822.

65 R. E. Nettleton and M. S. Green, *J. Chem. Phys.*, 1958, **29**, 1365–1370.

66 R. D. Mountain and H. J. Raveché, *J. Chem. Phys.*, 1971, **55**, 2250–2255.

67 T. B. Schrøder, N. Gnan, U. R. Pedersen, N. P. Bailey and J. C. Dyre, *The Journal of Chemical Physics*, 2011, **134**, –.

68 J. R. Seth, L. Mohan, C. Locatelli-Champagne, M. Cloitre and R. T. Bonnecaze, *Nat Mater*, 2011, **10**, 838–843.

69 S. R. Rastogi, N. J. Wagner and S. R. Lustig, *J. Chem. Phys.*, 1996, **104**, 9234–9248.

70 J. F. Morris and B. Katyal, *Phys. Fluids*, 2002, **14**, 1920–1937.